

**KERNFORSCHUNGSZENTRUM
KARLSRUHE**

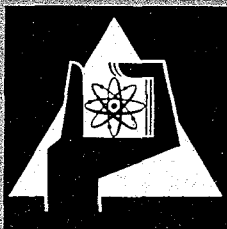
Januar 1967

KFK 507

Institut für Angewandte Reaktorphysik

Heterogeneity Effects in SNEAK Doppler Loop Measurements

W. K. Foell



GESELLSCHAFT FÜR KERNFORSCHUNG M. B. H.

KARLSRUHE

Als Manuskript vervielfältigt.

Für diesen Bericht behalten wir uns alle Rechte vor.

Gesellschaft für Kernforschung m. b. H.

Karlsruhe

KERNFORSCHUNGSZENTRUM KARLSRUHE

Januar 1967

KFK-507

Institut für Angewandte Reaktorphysik

Heterogeneity Effects in SNEAK Doppler Loop Measurements^{*)}

W.K. FOELL

Gesellschaft für Kernforschung mbH., Karlsruhe

^{*)} Work performed within the association in the field of fast reactors between the European Atomic Energy Community and Gesellschaft für Kernforschung mbH., Karlsruhe

A broad program of Doppler effect measurements is planned for SNEAK, the Karlsruhe fast critical assembly /1/. The experimental approach is intended to be very flexible so that the temperature effects can be measured over a wide range of temperatures, sample volumes, sample compositions, and core compositions. In addition to the usual small-sample pile oscillator measurements on $U^{238}O_2$ and PuO_2 , a Doppler "Loop" is planned in which hot gas is used to heat up as much as five liters of the center region of the SNEAK assembly /2/. This type of experiment, although perhaps lacking the extremely high precision of the small-sample measurement, has the advantage of yielding Doppler coefficients of the actual core composition, including structural and coolant materials.

The Doppler test zone will consist of 1, 4, or 9 modified SNEAK fuel elements which can be oscillated in temperatures between 300 and 650°K. In contrast to the normal platelet construction of the SNEAK elements, these elements will contain a quadratic array of cladded pins; the cladded pins are filled with the material necessary to achieve the desired overall test zone composition. Three basic pin compositions are planned: a) Fertile material; b) Fertile-fissile mixture; c) Structural and simulated coolant materials. The various combinations of these three pin types make possible a wide range of overall "homogenized" compositions.

The purpose of this note is to examine the heterogeneity effects arising from the separation of the materials in pins of finite **diameters**. The heart of the problem lies in the fact that the fertile material, U^{238} , is present in pins of both type a and b but in different concentrations. The fissile material, Pu^{239} , is present in pin type b only. Because the matrix of pins results in a rather complex geometry, the approach chosen was to study one of the most extreme cases, i.e., when the matrix consists of alternating rows of pin a and pin b, respectively. In such a case the system may be approximated rather well by an infinite array of one-dimensional slabs. The model and typical atom compositions are shown in Fig. 1. The structural and coolant materials of SNEAK 3 (mock up of a steam-cooled fast reactor) are lumped equally into each of the slabs.

The conventional first-flight collision probability equations can be written to describe the collision rate in each region j at lethargy u :

$$\sum_{tj}(u)\phi_j(u)V_j = \sum_{k=1}^2 P_{kj}(u)V_k \int \sum_{sk}(u' \rightarrow u)\phi_k(u')du', \quad (1)$$

where \sum_{tj} = total macroscopic cross section in region j;
 \sum_{sj} = macroscopic scattering cross section in region j;
 ϕ_j = neutron flux in region j;
 V_j = volume of region j;
 P_{kj} = probability that a neutron born in region k suffers its first collision in region j.

Invoking the narrow resonance approximation, and assuming that the scattering cross section between resonances is independent of lethargy, we can express the source as

$$\int \sum_{sk}(u' \rightarrow u)\phi(u')du' = \sum_{pk}\phi_o, \quad (2)$$

where \sum_{pk} = macroscopic potential scattering cross section in region k;
 ϕ_o = lethargy and space independent flux between resonances.

Equation (1) can then be written as

$$\sum_{tj}(u)\phi_j(u)V_j = \sum_{k=1}^2 P_{kj}(u)V_k \sum_{pk}\phi_o. \quad (3)$$

At this point, the reciprocity theorem is introduced. Within the limits of the flat source approximation, it can be expressed as

$$P_{jk}(u)\sum_{tj}(u)V_j = P_{kj}(u)\sum_{tk}(u)V_k. \quad (4)$$

The combination of (3) and (4) results in

$$\phi_j(u) = \phi_o \sum_{k=1}^2 P_{jk}(u) \frac{\sum_{pk}}{\sum_{tk}(u)} \quad (5)$$

Using Eqn. (5) and the fact that $P_{11} = 1 - P_{12}$, the fluxes in regions 1 and 2 may be expressed explicitly as (for convenience, the lethargy argument will be dropped)

$$\phi_1 = \phi_o \left\{ \frac{\overline{\sigma}_{p1}}{\overline{\sigma}_{t1}} + P_{12} \left[\frac{\overline{\sigma}_{p2}}{\overline{\sigma}_{t2}} - \frac{\overline{\sigma}_{p1}}{\overline{\sigma}_{t1}} \right] \right\} \quad (6)$$

and

$$\phi_2 = \phi_o \left\{ \frac{\overline{\sigma}_{p2}}{\overline{\sigma}_{t2}} + \frac{V_1 N_1}{V_2 N_2} P_{12} \left[\frac{(\overline{\sigma}_{p1} - \overline{\sigma}_{p2})}{\overline{\sigma}_{t2}} - \frac{\overline{\sigma}_{p2}(\overline{\sigma}_{p1} - \overline{\sigma}_{p2})}{(\overline{\sigma}_{t2})^2} \right] \right\}. \quad (7)$$

Here the microscopic cross sections are in terms of barns per absorber atom; and the total cross section is expressed as the sum of the potential and resonance contributions, i.e.,

$$\bar{\sigma}_t = \bar{\sigma}_r + \bar{\sigma}_p.$$

The reaction rate of the resonance absorber, e.g., the absorption in region 1 due to a U238 resonance, is

$$R_{a1}^8 = N_1^8 V_1 \phi_0 \int_{\text{Res}} \left\{ \frac{\sigma_a^8 \bar{\sigma}_{p1}}{\bar{\sigma}_{t1}} + P_{12} \left[\frac{\sigma_a^8 \bar{\sigma}_{p2}}{\bar{\sigma}_{t2}} - \frac{\sigma_a^8 \bar{\sigma}_{p1}}{\bar{\sigma}_{t1}} \right] \right\}, \quad (8)$$

where the subscript "a" signifies absorption.

The escape probability P_{12} for the infinite array of slabs can be expressed in terms of P_{11}^0 , the collision probability for a single slab in an infinite medium (e.g. see /3/).

$$\begin{aligned} P_{12} &= (1-P_{11}^0) \left[(1-T_2) + T_2 T_1 (1-T_2) + (T_2 T_1)^2 (1-T_2) + \dots \right] \\ &= (1-P_{11}^0)(1-T_2) \sum_{n=0}^{\infty} (T_1 T_2)^n = \frac{(1-P_{11}^0)(1-T_2)}{1-T_1 T_2}, \end{aligned} \quad (9)$$

where T_1 and T_2 are the first-flight transmission probabilities for slabs 1 and 2 respectively. If it is assumed that the neutrons are impinging upon the slabs with random orientation, these transmission probabilities may be expressed as (see /3/)

$$T_1 = 1 - 2 \sum_{t1} d_1 (1-P_{11}^0) \quad (10)$$

and
$$T_2 = 1 - 2 \sum_{t2} d_2 (1-P_{22}^0) \quad (11)$$

where P_{11}^0 and P_{22}^0 are the first-flight collision probabilities for isolated slabs 1 and 2 respectively, and d is the slab thickness. These latter probabilities are tabulated in /4/.

Equations (9), (10), and (11) could then be substituted into (8), and the reaction rate could be evaluated by means of a numerical integration over the resonance line shapes. If the resonance cross sections in a portion of the energy range are unresolved, the integration must also be carried out over a statistical distribution of resonance parameters. To avoid these tedious numerical integrations, a finite sum of rational functions, as first suggested by D. Wintzer /5/, has been used to approximate the P_{12} functions. The use of these

rational functions results in an expression for the reaction rates which contains the usual "J-Functions". These functions are used for the calculation of resonance integrals of homogeneous systems and have been extensively tabulated, e.g., /6/. The technique is outlined below, as applied to the U238 reaction rate calculation.

The total cross section of each region is expressed as a sum of U238 resonance cross section, i.e., σ_r^8 , and total non-resonance cross section.

$$\Sigma_{t1} = N_1^8 \sigma_r^8 + \Sigma_{p1} \quad (12)$$

$$\Sigma_{t2} = N_2^8 \sigma_r^8 + \Sigma_{p2} \quad (13)$$

The escape probability, P_{12} , is then calculated from Eqn. (9) for several values of σ_r^8 within the range, 0 - 5000 barns, a range appropriate for the U238 resonances in the energy range most important to the Doppler effect. These resulting values of P_{12} are then fitted, using a least-squares technique, to a function of the form

$$P_{12} = \sum_{\nu=1}^M \frac{a_{\nu}}{\sigma_r^8 + b_{\nu}} \quad (14)$$

where the b_{ν} values are chosen, and the a_{ν} values are parameters determined by the fitting technique. Experience has shown that, with a reasonable number and choice of b_{ν} values (5 to 10 values are usually adequate), the fitted and calculated curves deviate less than 1% from each other.

The substitution of (14) in (8) gives

$$R_{a1}^8 = N_1^8 V_1 \phi_0 \left\{ \int_{\text{Res}} \frac{\sigma_a^8 \sigma_{p1}}{\sigma_r^8 + \sigma_{p1}} + \sum_{\nu=1}^M \frac{a_{\nu}}{\sigma_r^8 + b_{\nu}} \left[\frac{\sigma_a^8 \sigma_{p2}}{\sigma_r^8 + \sigma_{p2}} - \frac{\sigma_a^8 \sigma_{p1}}{\sigma_r^8 + \sigma_{p1}} \right] \right\} \quad (15)$$

The last two terms of (15) are expanded by means of partial fractions, yielding

$$R_{a1}^8 = N_1^8 V_1 \phi_0 \left\{ \int_{\text{Res}} \frac{\sigma_{p1} \sigma_a^8}{\sigma_r^8 + \sigma_{p1}} + \sum_{\nu=1}^M \left[\frac{\sigma_{p1}}{\sigma_{p1} - b_{\nu}} \frac{\sigma_a^8}{\sigma_r^8 + \sigma_{p1}} - \frac{\sigma_{p2}}{\sigma_{p2} - b_{\nu}} \frac{\sigma_a^8}{\sigma_r^8 + \sigma_{p2}} + \frac{b_{\nu}(\sigma_{p1} - \sigma_{p2})}{(\sigma_{p2} - b_{\nu})(\sigma_{p1} - b_{\nu})} \frac{\sigma_a^8}{\sigma_r^8 + b_{\nu}} \right] \right\} \quad (16)$$

If now, ψ , the usual single-level Doppler-broadened line shape, is introduced for σ_r^0 , we obtain

$$R_{a1}^0 = N_1^0 V_1 \phi_0 \left\{ \sigma_{p1} \Gamma_\gamma \int_0^\infty \frac{\psi}{\psi+B_1} dx + \sum_{\nu=1}^M a_\nu \left[\frac{\sigma_{p1}}{\sigma_{p1}-b_\nu} \Gamma_\gamma \int_0^\infty \frac{\psi}{\psi+B_1} dx - \frac{\sigma_{p2}}{\sigma_{p2}-b_\nu} \Gamma_\gamma \int_0^\infty \frac{\psi}{\psi+B_2} dx + \frac{b(\sigma_{p1}-\sigma_{p2})}{(\sigma_{p1}-b_\nu)(\sigma_{p2}-b_\nu)} \Gamma_\gamma \int_0^\infty \frac{\psi}{\psi+B_\nu} dx \right] \right\} \quad (17)$$

$$= N_1^0 V_1 \phi_0 \left\{ \sigma_{p1} \Gamma_\gamma J(B_1) + \sum_{\nu=1}^M a_\nu \left[\frac{\sigma_{p1}}{\sigma_{p1}-b_\nu} \Gamma_\gamma J(B_1) - \frac{\sigma_{p2}}{\sigma_{p2}-b_\nu} \Gamma_\gamma J(B_2) + \frac{b(\sigma_{p1}-\sigma_{p2})}{(\sigma_{p1}-b_\nu)(\sigma_{p2}-b_\nu)} \Gamma_\gamma J(B_\nu) \right] \right\}, \quad (18)$$

where $J(B) = \int_0^\infty \frac{\psi}{\psi+B} dx$

and B is the ratio of non-resonant to peak resonance cross section. If the resonances are unresolved, $J(B)$ must be averaged over a distribution of neutron widths, i.e.,

$$R_{a1}^0 = N_1^0 V_1 \phi_0 \left\{ \frac{\sigma_{p1} \Gamma_\gamma \langle J(B_1) \rangle}{\langle S \rangle} + \sum_{\nu=1}^M a_\nu \left[\frac{\sigma_{p1}}{\sigma_{p1}-b_\nu} \Gamma_\gamma \frac{\langle J(B_1) \rangle}{\langle S \rangle} - \frac{\sigma_{p2}}{\sigma_{p2}-b_\nu} \Gamma_\gamma \frac{\langle J(B_2) \rangle}{\langle S \rangle} + \frac{b_\nu(\sigma_{p1}-\sigma_{p2})}{(\sigma_{p1}-b_\nu)(\sigma_{p2}-b_\nu)} \Gamma_\gamma \frac{\langle J(B_\nu) \rangle}{\langle S \rangle} \right] \right\}, \quad (19)$$

where $\langle J \rangle = \int_0^\infty d\Gamma_n P(\Gamma_n) \int_0^\infty \frac{\psi}{\psi+B} dx;$

$\langle S \rangle$ = the average level spacing;

and $P(\Gamma_n)$ = is a probability distribution of the neutron widths.

In a similar manner, the absorption reaction rate of the U238 in region 2 can be expressed as

$$R_{a2}^0 = N_2^0 V_2 \phi_0 \left\{ \sigma_{p2} \Gamma_\gamma \frac{\langle J(B_2) \rangle}{\langle S \rangle} + \frac{V_1 N_1}{V_2 N_2} \sum_{\nu=1}^M a_\nu \frac{b(\sigma_{p2}-\sigma_{p1})}{(\sigma_{p2}-b_\nu)^2} \left[\Gamma_\gamma \frac{\langle J(B_\nu) \rangle}{\langle S \rangle} - \Gamma_\gamma \frac{\langle J(B_2) \rangle}{\langle S \rangle} \right] + \frac{\sigma_{p2}(\sigma_{p2}-\sigma_{p1})}{(\sigma_{p2}-b_\nu)} \Gamma_\gamma \frac{\langle J(B_2) \rangle}{\langle S \rangle} \right\} \quad (20)$$

where $J'(\beta)$ is related to the derivative of the J-function by

$$J' = \int_0^{\infty} \frac{\psi^2}{(\psi+\beta)^2} dx = J + \sigma_p \frac{\partial J}{\partial \sigma_p}.$$

Equations (19) and (20) give the reaction rates for regions 1 and 2 in terms of a simple sum of averaged $J(\beta)$ functions.

It is seen that (19) and (20) approach the correct limit of the homogeneous case when $\sigma_{p2} \rightarrow \sigma_{p1}$. In addition it can easily be verified that if $N_2 \rightarrow 0$, and P_{12} is expressed by the Wigner Rational Approximation,

$$P_{12} = \frac{a}{\sigma_{g+b}} = \frac{\frac{1}{\bar{L}_1 N_1}}{\sigma_g + (\sigma_{p1} + \frac{1}{\bar{L}_1 N_1})}$$

where \bar{L}_1 = the average chord length in region 1, then R_{a1}^g approaches the limit given by the equivalence theorem /6/, i.e.,

$$R_{a1}^g = N_1 V_1 \phi_0 \sigma_p \bar{\gamma} \frac{\langle J(\beta^*) \rangle}{\langle S \rangle}, \quad (21)$$

$$\text{where } \sigma_p^* = \sigma_{p1} + \frac{1}{\bar{L}_1 N_1}.$$

An alternative approach to the evaluation of Eqn. 7 is to express P_{12}/σ_{t2} as a sum of rational functions. Equation 14 is then replaced by

$$\frac{P_{12}}{\sigma_{t2}} = \sum_{\nu=1}^M \frac{a_{\nu}}{\sigma_{r+b_{\nu}}}. \quad (22)$$

This leads to the following expressions for the reaction rates:

$$R_{a1}^g = N_1^g V_1 \phi_0 \left\{ \sigma_{p1} \bar{\gamma} \frac{\langle J(\beta_1) \rangle}{\langle S \rangle} + \sum_{\nu=1}^M a_{\nu} \left[\frac{(\sigma_{p2} - \sigma_{p1})}{(\sigma_{p1} - b_{\nu})} \left[\sigma_{p1} \bar{\gamma} \frac{\langle J(\beta_1) \rangle}{\langle S \rangle} - b_{\nu} \bar{\gamma} \frac{\langle J(\beta_{\nu}) \rangle}{\langle S \rangle} \right] \right] \right\} \quad (23)$$

$$R_{a2}^g = N_2^g V_2 \phi_0 \left\{ \sigma_{p2} \bar{\gamma} \frac{\langle J(\beta_2) \rangle}{\langle S \rangle} + \frac{V_1 N_1}{V_2 N_2} \sum_{\nu=1}^M a_{\nu} \left[\frac{(\sigma_{p1} - \sigma_{p2})}{(\sigma_{p2} - b_{\nu})} \left[\sigma_{p2} \bar{\gamma} \frac{\langle J(\beta_2) \rangle}{\langle S \rangle} - b_{\nu} \bar{\gamma} \frac{\langle J(\beta_{\nu}) \rangle}{\langle S \rangle} \right] \right] \right\} \quad (24)$$

It is seen that Eqn.(24) does not contain the derivative function that is present in Eqn.(20); because of the limited accuracy of the available J'-functions, Eqn (24) has given better results in some cases. In general, however, the two methods give the same reaction rates.

Typical Numerical Results

Earlier calculations for a homogeneous SNEAK 3 system have shown that the Doppler effect peaks at about 500 eV, with the majority of it occurring between 100 and 1000 eV. Equations (19) and (20) or Eqns. (23) and (24) have therefore been evaluated for the U238 and Pu239 in the system of Figure 1 at temperatures of 300 and 700°K, energies of 100, 500, and 1000 eV, and for slab thicknesses ranging from 0.01 to 10 cm. The cross section data used is given in Table 1. Computer codes written by A. Döderlein and D.K. Lorenz /7/ were used to calculate the required averages over the J-function.

Typical results for U238 are given in Fig. 2. For extremely thin slabs, the individual region reaction rates are proportional to the respective absorber atom densities, and their sum is equal to that in the homogeneous system. For the very thick slabs, the absorption rates approach the correct limits expected for slabs of infinite thickness. For slabs of finite thickness, the reaction rates exhibit a reasonable behavior as the thickness varies, i.e., the mutual effects of the respective sources, $\phi_1 \sigma_{p1}$ and $\phi_2 \sigma_{p2}$, decreases as the thickness increases. At a given temperature the total absorption rate is practically constant for all slab thicknesses. In addition, the difference between the total absorption rates at 300 and 700°K varies less than one percent for all thicknesses. This is primarily due to the fact that the macroscopic cross section and U238 density of the two regions do not greatly differ.

Typical results for the Pu239 absorption reaction rate at $E=500$ eV, and $T=300$ and 700°K are shown in Figure 3. The heterogeneity effect is greater than for U238, and for a feasible slab thickness of 1 cm, amounts to approximately 3 percent. Because Pu239 is present in region 2 only, it was also possible to calculate the absorption rate using the Bell approximation /8/. The results deviate considerably from the present treatment, and at $d=1$ cm, the Bell method overestimates by about 30% the effect of heterogeneity on absorption rate. Figure 4

shows the difference between Pu239 absorption rates at 300 and 700°K. At d=1 cm, this difference for the heterogeneous case is 6% larger than for the corresponding homogeneous case. The Bell method again overestimates the effect due to heterogeneity.

For the above calculations, the coolant and structural materials were distributed equally between the two regions. In practice most of the steel (which is the largest contributor to Σ_{p1} and Σ_{p2}) will be concentrated in pin cladding. To test the effect of this homogenization, the most extreme case, in which all of the steel was lumped into region 2, was studied. The results gave heterogeneity effects somewhat larger than those shown in Figure 2, but at realistic pin diameters, the heterogeneity effects amounted to only a few percent.

Because of heat transfer and cost considerations, the diameter for the pins in the Doppler loop will lie between 0.5 and 1 cm. The calculation of the approximate change in $\delta k/k$ caused by the heterogeneous structure requires the weighting of capture and fission reaction rates with the appropriate energy dependent adjoint functions and source densities. The above calculations show, however, that for such diameters, the measured Doppler effect should be very close to that of the homogeneous system.

Acknowledgements

The author is indebted to D. Wintzer for his suggestions and assistance with the collision probability calculations. Mr. A. Wickenhäuser and Mrs. I. Braun kindly carried out the necessary numerical work.

References

- /1/ P. ENGELMANN et al.: Construction and Experimental Equipment of the Karlsruhe Fast Critical Facility SNEAK, KFK-471
- /2/ P. ENGELMANN et al.: Initial Experiments in the Karlsruhe Fast Critical Facility SNEAK, KFK-472
- /3/ W. ROTHENSTEIN, Nucl.Sci.Eng. 7, 162-171 (1960)
- /4/ K.M. CASE et al.: Introduction to the Theory of Neutron Diffusion, I, Los Alamos Scientific Laboratory (1953)
- /5/ D. WINTZER, Institut für Angewandte Reaktorphysik, Kernforschungszentrum Karlsruhe, Personal Communication (May 1965)
- /6/ L. DRESNER: Resonance Absorption in Nuclear Reactors, Pergamon Press, London and New York (1960)
- /7/ A. DÖDERLEIN et al.: Berechnung der Resonanz-Selbstabschirmung in Gruppenkonstanten schneller Reaktoren, PSB-Bericht 116, Kernforschungszentrum Karlsruhe (1964)
- /8/ G.I. BELL, Nucl.Sci.Eng. 5, 75 (1959)

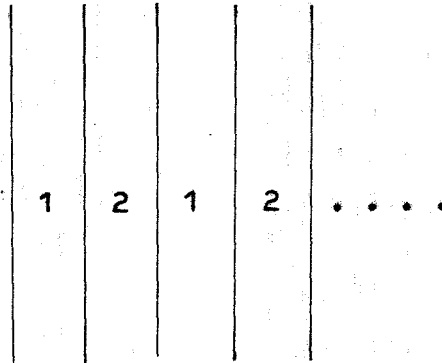
Table 1:

<u>U238</u>	$\langle \Gamma_n^0 \rangle$	$= 1.76 \times 10^{-3} (\text{eV})^{1/2}$	$\sigma_{p1} = 47.87 \text{ b}$
	Γ_γ	$= 24.6 \times 10^{-3} \text{ eV}$	$\sigma_{p2} = 63.83 \text{ b}$
	S	$= 18.5 \text{ eV}$	
<u>Pu239</u>	J=0: $\langle \Gamma_n^0 \rangle$	$= 0.98 \times 10^{-3} (\text{eV})^{1/2}$	$\langle S \rangle = 10.1 \text{ eV}$
	J=1: $\langle \Gamma_n^0 \rangle$	$= 0.326 \times 10^{-3} (\text{eV})^{1/2}$	$\langle S \rangle = 3.36 \text{ eV}$
	Γ_γ	$= 39 \times 10^{-3} \text{ eV}$	$\langle \Gamma_f \rangle = 98 \times 10^{-3} \text{ eV}$
	σ_{p2}	$= 191.5 \text{ b}$	

List of Figures

1. Two Region, Infinite Array-Model of SNEAK Doppler Loop
2. U238 Absorption Rates in Regions 1 and 2 of SNEAK Doppler Loop
3. Pu239 Absorption Rate in SNEAK Doppler Loop
4. Difference between Pu239 Absorption Rates at $T=300$ and 700°K

Figure 1:



Region 1

$N_8 = 8.92 \times 10^{21}$ nuclei/cm³
 $N_H = 1.64$ "
 $N_{ox} = 18.76$ "
 $N_{Fe} = 20.5$ "

Region 2

$N_8 = 6.69 \times 10^{21}$ nuclei/cm³
 $N_9 = 2.23$ "
 $N_H = 1.64$ "
 $N_{ox} = 18.76$ "
 $N_{Fe} = 20.5$ "

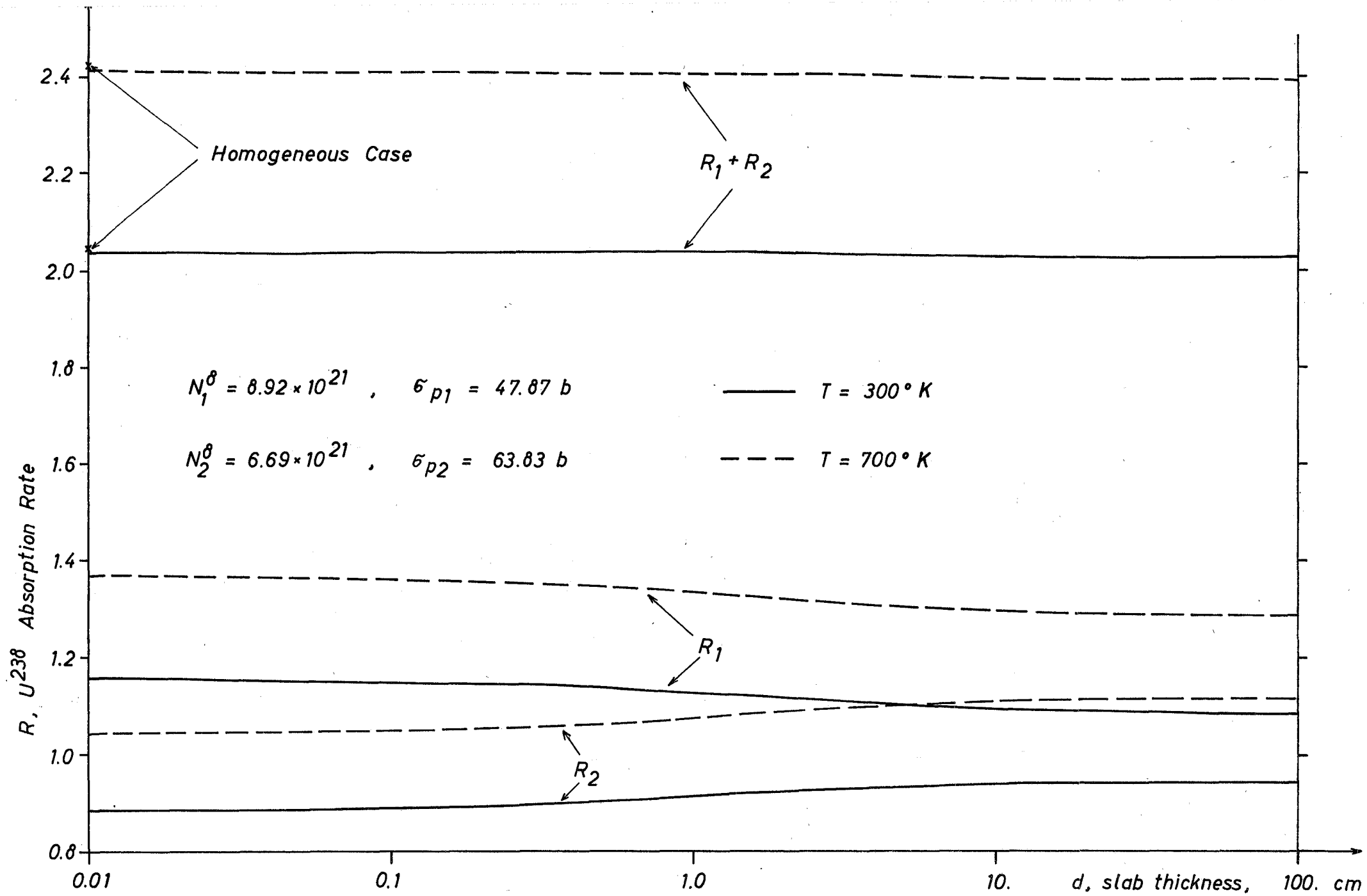


Fig. 2

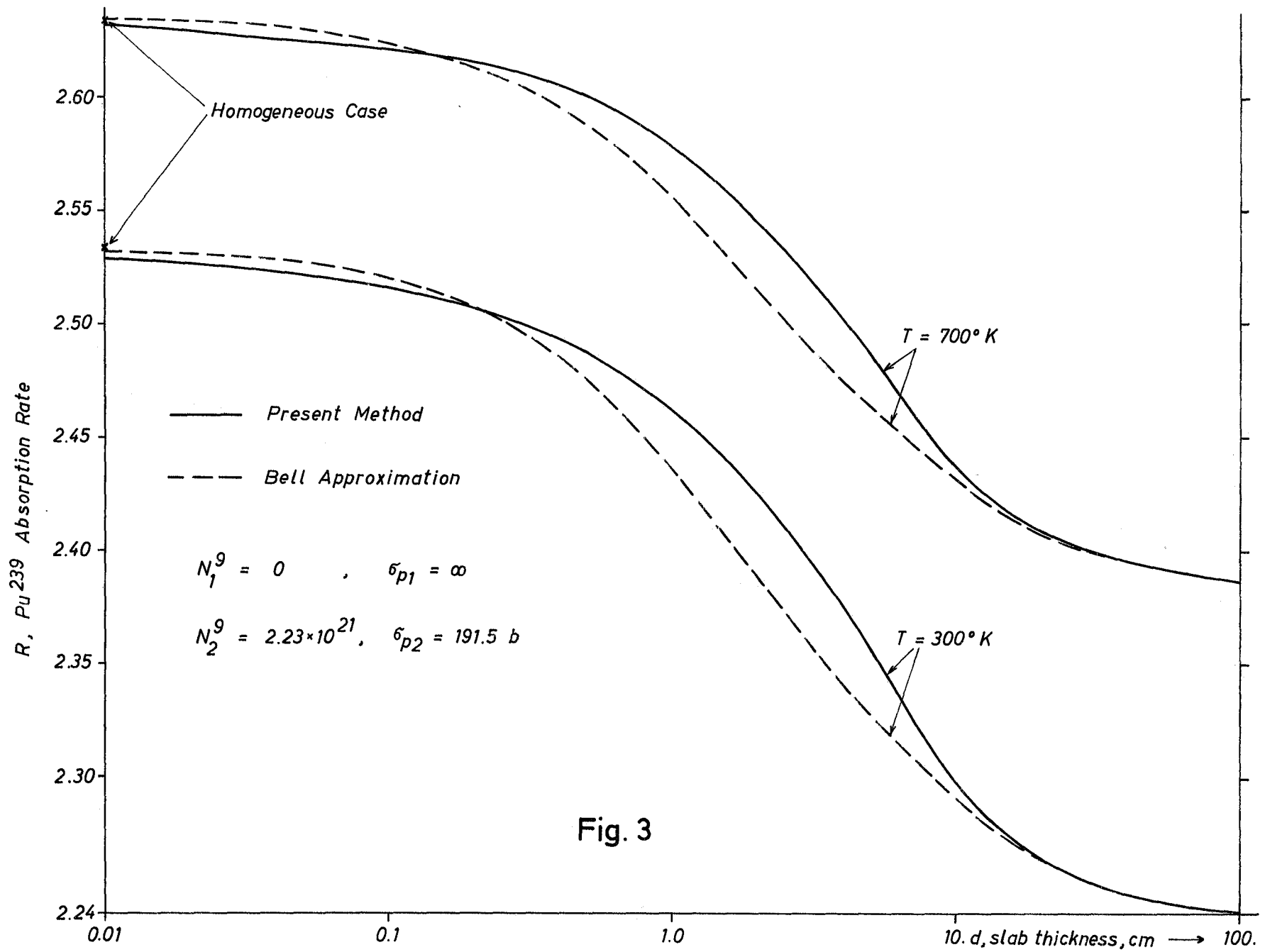


Fig. 3

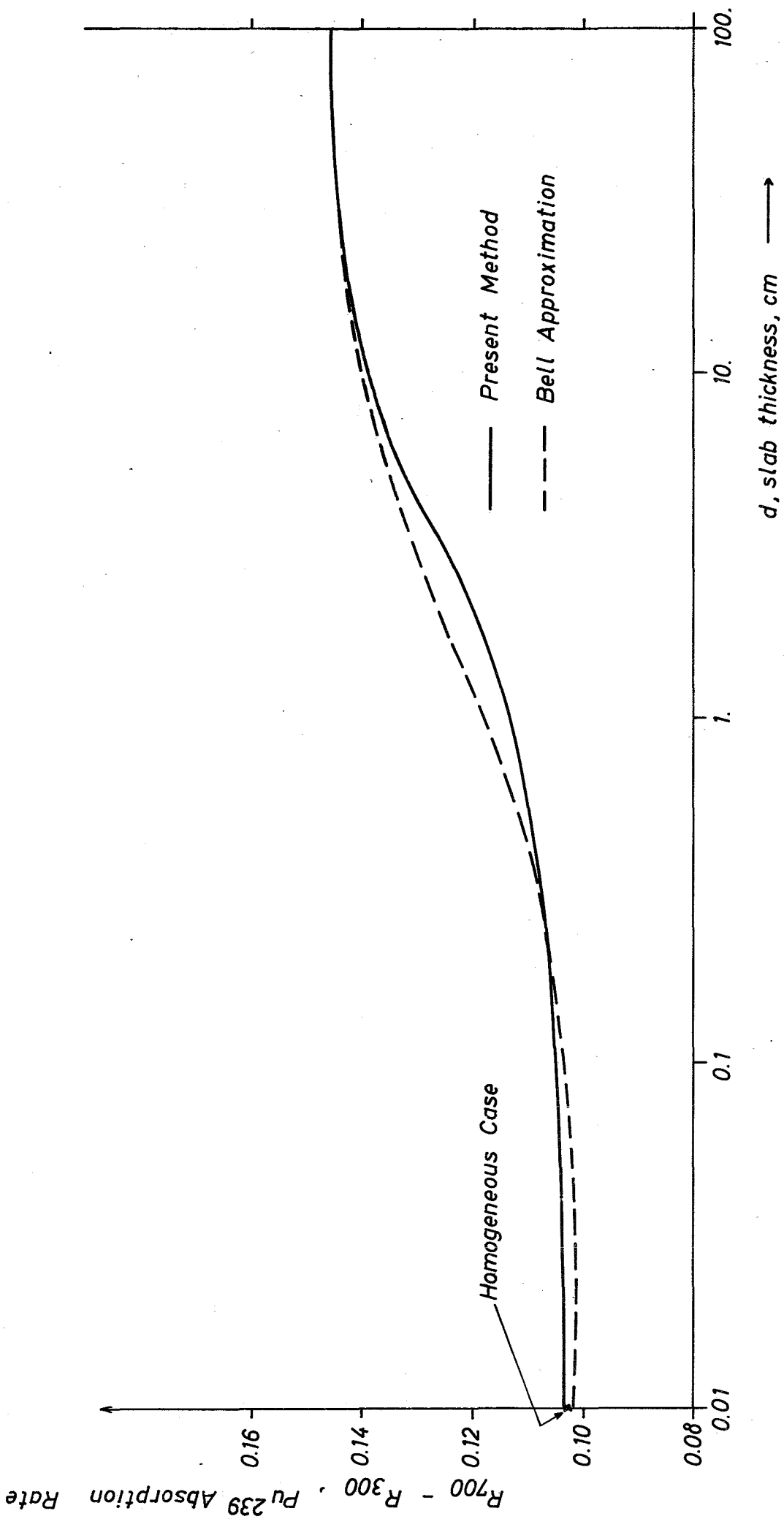


Fig. 4